Hindawi
Advances in Civil Engineering
Volume 2022, Article ID 5760913, 15 pages
https://doi.org/10.1155/2022/5760913

Research Article

A Method for Rapidly Determining the Seismic Performance of Buildings Based on Remote-Sensing Imagery and Its Application

Sihan Yu,[1] Xiaofeng Xie,[1] Peng Du,[1] Xiaoqing Wang,[2] Shun Yang,[1] and Chao Liu[1]

[1]*Earthquake Agency of Ningxia Hui Autonomous Region, Yinchuan 750001, China*
[2]*Institute of Earthquake Science, China Earthquake Administration, Beijing 100036, China*

Correspondence should be addressed to Xiaofeng Xie; feashange@126.com

Received 14 May 2022; Revised 11 August 2022; Accepted 17 September 2022; Published 3 October 2022

Academic Editor: Fadzli Mohamed Nazri

Remote-sensing images are visually interpreted in this study to obtain information on buildings in the urban and rural areas of Ningxia, China. Overall, area estimates yielded by the proposed equations followed a normal distribution. Correlation and error analyses indicated that the coefficients are reasonable and reliable and that the building area estimates have an accuracy of 90% and are also reliable. These results were used in conjunction with drone aerial images, Baidu street view images, and paper maps to determine the seismic performance (SP) of the buildings in the study area. On this basis, the buildings were classified into three groups, namely, those with the required SP, suspected substandard SP, and substandard SP. Examination based on the field survey data collected from at least one sample site in each village and township in all 22 county-level divisions (CLDs) of Ningxia showed an average SP accuracy of 76% for all 22 CLDs and an SP accuracy exceeding 70% for 20 (91%) of the 22 CLDs. Based on this approach and the results obtained, the ArcGIS spatial analysis method was employed to determine the percentages and distribution patterns of the buildings in the three SP groups in the 22 CLDs. The results revealed the following features. Buildings with the required SP were clustered in the urban areas of each CLD, with a few in the village and township government seats. Buildings with suspected substandard SP were distributed predominantly in the rural-urban fringe (RUF) areas and the village and township government seats. Buildings with substandard SP were found primarily in urban villages, RUF areas, and urban areas. The soundness of the spatial analysis results was corroborated by the field survey data, lending credence to the feasibility of the proposed calculation method. This method can satisfy the real-world need for rapidly assessing the SP and distribution of buildings in a region before an earthquake occurs and provide a reliable reference for disaster prevention, mitigation, and relief efforts.

1. Introduction

Earthquakes are unpredictable and highly destructive natural disasters that gravely threaten social and economic development, the safety of lifeline facilities, and people's lives and property [1]. Rapid economic progress and accelerated urbanisation have broadened and deepened the impact of destructive earthquakes on urban development in China.

Aboveground structures often suffer damage and even collapse during destructive earthquakes, constituting the principal cause of casualties and property losses. Massive volumes of building data considerably affect the timeliness and accuracy of rapid damage assessments after strong earthquakes. Generally, postdisaster building damage can be assessed through either a detailed field investigation of the damage sustained by individual buildings or the determination of the damage sustained by buildings over a large area using an efficient analysis method [2]. Findings from available studies suggest that the number of buildings within an assessment zone increases exponentially as the earthquake magnitude increases [3]. Field investigations are time- and labour-intensive and thus unsuitable for assessing damage over a large area after a strong earthquake [4]. Hence, the focus of research examining earthquake damage has gradually shifted from postearthquake investigations to preearthquake disaster mitigation preparations. Well-prepared emergency management strategies can alleviate the losses from earthquakes [5].

Because of its ability to provide timely, multipurpose, multiangle image-based services, remote-sensing (RS)

technology has become a convenient tool for obtaining information before and after an earthquake and facilitating postearthquake emergency response and recovery efforts. The earliest use of RS technology to acquire earthquake damage information dates back to 1906 when G. R. Lawrence photographed San Francisco in the United States after a magnitude-8.3 earthquake using kites. Technological advances have enabled substantial progress in RS technology in recent decades. With higher resolutions and update rates, satellite images can now better facilitate assessment of the damage caused by historical earthquakes and the acquisition of earthquake damage information. A growing number of researchers have retrieved information on the damage sustained by buildings over large areas during earthquakes from RS imagery [4, 6–17]. Satellite RS technology has become a convenient and efficient tool for obtaining and disseminating information before and after earthquakes, facilitating a more effective emergency response to earthquakes and minimising their impact. Swiftly understanding the seismic performance (SP) of buildings in an earthquake-prone area before the occurrence of an earthquake plays a crucial role in urban disaster mitigation and emergency rescue efforts.

In this study, using the Seismic Ground Motion Parameter Zonation Map of China (GB18306-2015) [18] and the Code for Seismic Design of Buildings (GB50011-2016) [19] as guidelines, urban and rural buildings in Ningxia, China, were preliminarily classified based on their SP through visual interpretation of high-resolution RS imagery into three groups (termed SP groups), namely, those with the required SP, suspected substandard SP, and substandard SP. The reliability of the results obtained based on visual interpretation is comprehensively examined using drone aerial images, Baidu street view images, and paper maps. However, visual interpretation of RS imagery can only yield the number of buildings and cannot give the area of the buildings in each SP group. Therefore, a method must be established to determine the total area of the buildings in each of the three SP groups and its percentage in a region, with the goal of effectively mitigating earthquake damage. Rural and urban buildings are separately classified in this study. Separate equations are established to calculate the areas of rural and urban buildings. Error analysis revealed a high level of consistency between the building areas determined based on field survey data and rapidly yielded by the models. Within a permissible error range, the calculation models can be used to quickly estimate building areas in a region. On this basis, together with the SP estimates, the proportions of buildings with different SP levels and the distribution pattern of SP in a region can be determined. This method can provide powerful support for obtaining building information for an earthquake-prone region and estimating potential economic losses before an earthquake.

2. Study Area and Image Interpretation

2.1. Study Area. In terms of the geological structure, Ningxia is situated on the northeastern margin of the Tibetan Plateau, where active faults are densely distributed. According to historical records, this region has experienced multiple strong earthquakes, including two earthquakes with a magnitude of 8 and above: the magnitude-8 earthquake that occurred in Pingluo, Yinchuan, in 1739 and the magnitude-8.5 earthquake that occurred in Haiyuan in 1920. Modern instrumental records also show that Ningxia is prone to earthquakes. Figure 1 shows the study area.

2.2. Image Interpretation. Gaofen-2 imagery is used for analysis in this study. Its high spatial resolution (>1 m) meets the requirement for visual interpretation and allows aboveground structures to be quickly classified based on their SP. Considering its offsets, the geographical information system method is employed to correct the position coordinates in the Gaofen-2 imagery in the ArcGIS platform prior to visual interpretation [20].

The Seismic Ground Motion Parameter Zonation Map of China (GB18306-2015) and the Standard for Classification of Seismic Protection of Building Constructions (GB50223-2008) [21] are used in this study as a basis for determining building SPs. To relatively accurately distinguish building SPs, urban and rural buildings are processed separately during visual interpretation. The outlines of urban buildings are extracted individually based on their image texture. In other words, one polygon corresponds to one building. In contrast, the outlines of rural buildings are extracted based on the outlines of the blocks where they are located. In other words, one polygon can contain one or multiple buildings. Figure 2 illustrates the overall process used to determine building SPs and validate the results based on field survey data. Figure 3 shows separate standard maps of building outline information for urban and rural areas.

The Code for Seismic Design of Buildings (GB50011-2016) stipulates three fortification levels, that is, "no damage under minor earthquake," "repairable damage under moderate earthquake," and "no collapse under major earthquake." The degree of damage to buildings is qualitatively classified in the Classification of Earthquake Damage to Buildings and Special Structures (GB/T 24335-2009) [22]. According to the Seismic Ground Motion Parameter Zonation Map of China (GB18306-2015), Ningxia is mainly located in seismic fortification area VIII. In this study, the buildings in Ningxia are divided into three categories, namely, buildings with the required SP, suspected substandard SP, and substandard SP, according to the seismic standard for seismic fortification area VIII and with reference to the above two specifications.

Visually interpreting images of urban buildings is relatively easy. A building is considered to meet the SP standard if its polygon has a well-defined texture boundary. Buildings whose polygons have an indistinct or dark grey texture boundary are mostly structures consisting of 3–5 storeys and are suspected to be below the SP standard. Buildings lacking the above features and whose polygons are appreciably smaller than those of the buildings in the above two groups are mostly structures in urban villages and are considered to be below the SP standard. Using Baidu street view images

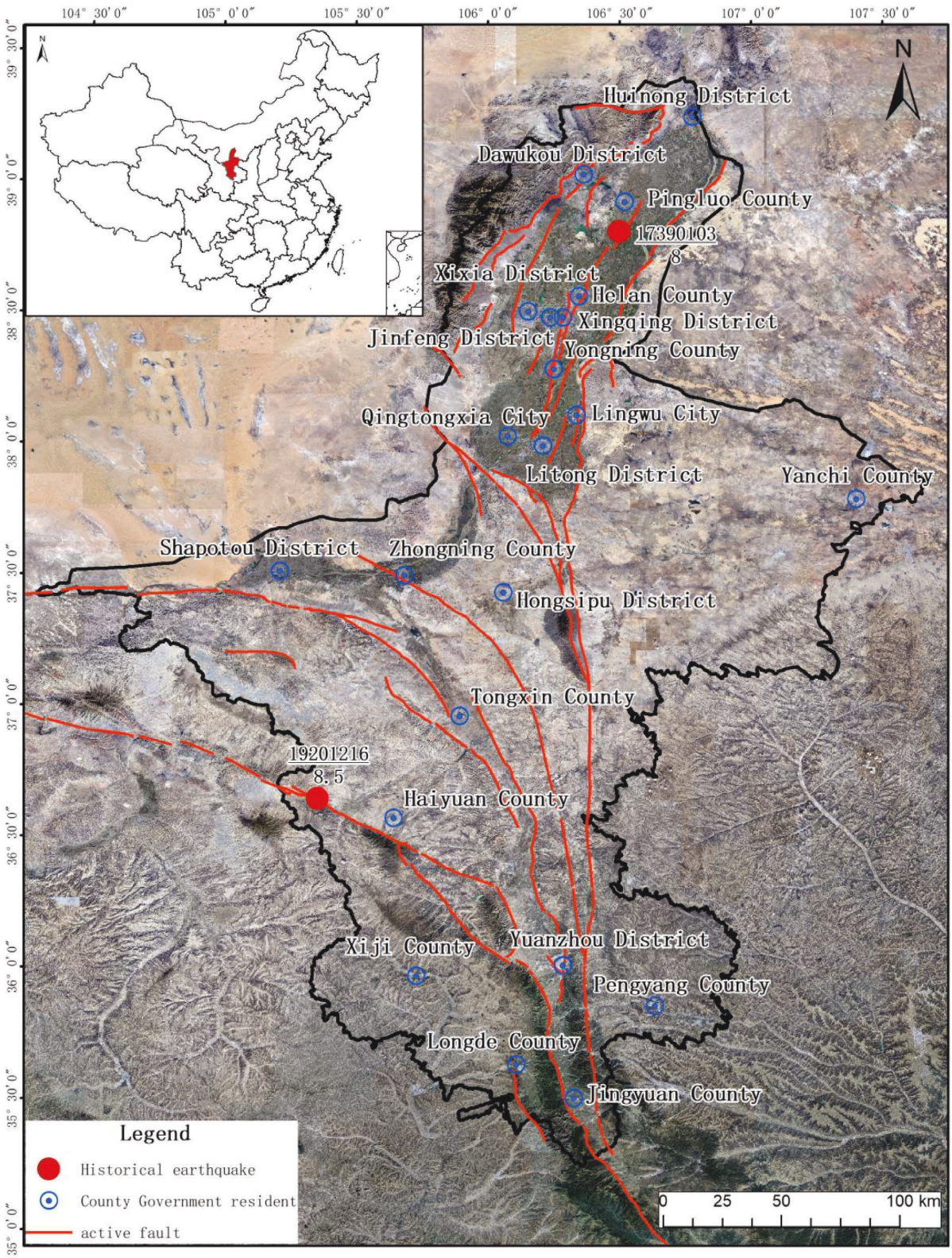

Figure 1: Study area.

can help determine the SP of individual buildings that appear to be ambiguous based on the information extracted from the RS images.

Rural and rural-urban fringe (RUF) areas are home to buildings of complex and varied structures and types. Therefore, a uniform standard for determining the SP of

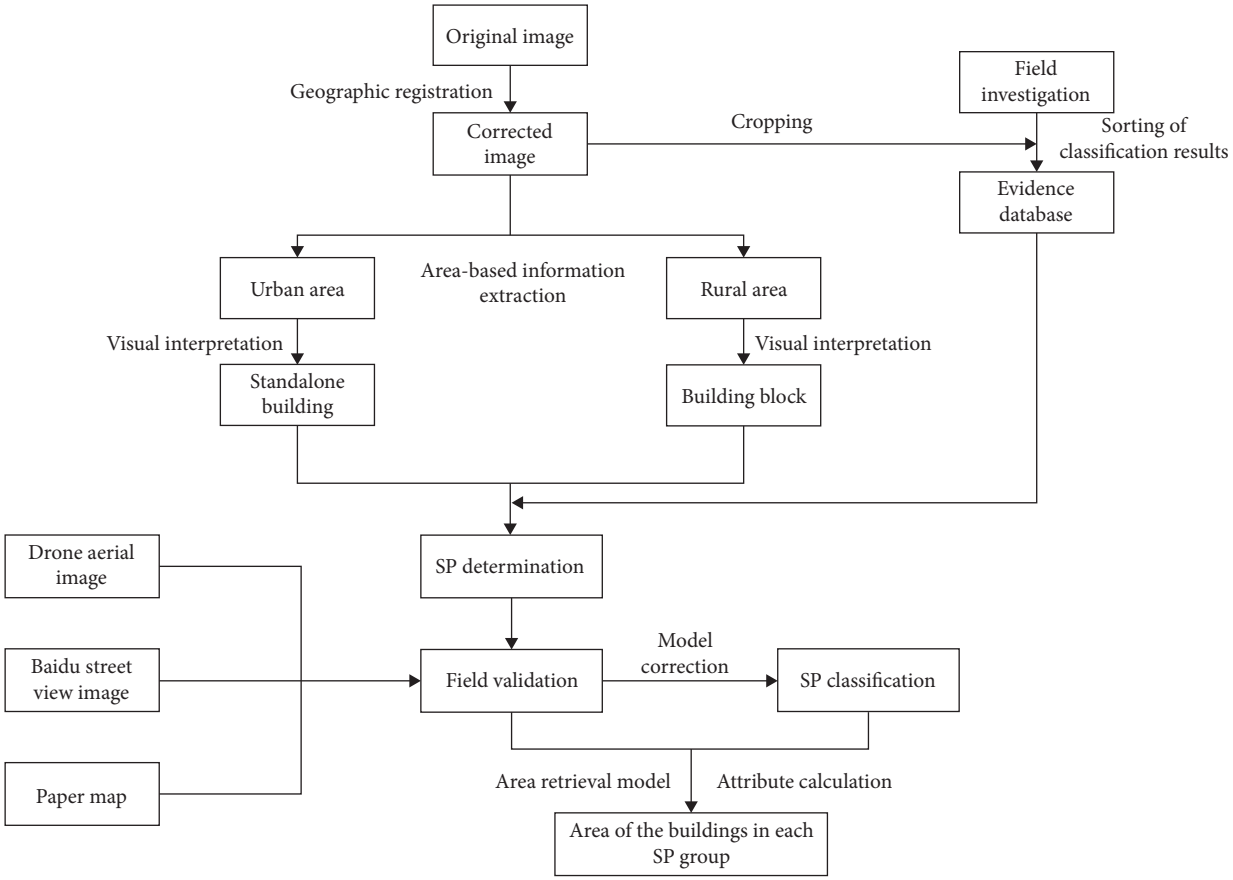

Figure 2: Flowchart of the method for visually interpreting the RS imagery and SP correction.

(a) (b)

Figure 3: Standard maps of extracted building information for (a) an urban area and (b) a rural area.

buildings needs to be established to facilitate laboratory visual interpretation. Prior to visual interpretation, field surveys were conducted to determine the typical features of the buildings in representative areas identified in the RS images. It is difficult to visually interpret RS images for buildings in rural and RUF areas and to extract their information (e.g., geometries and roof and shadow features) from RS images. Considering these factors in conjunction with field sample survey data, buildings in rural and RUF areas are classified based on their SP into three groups. The classification criteria, as shown in Figure 4, are described as follows:

(1) Buildings designed and constructed in rural areas by their owners themselves lack a uniform plan and layout and display various texture patterns and colours in the RS images. These buildings are classified as self-constructed (SC) buildings in rural areas. Field surveys

Figure 4: Typical buildings in rural and RUF areas.

show that most SC buildings are not seismically fortified and do not meet the SP standard. In the RS images, these buildings feature blurry texture boundaries and are mostly dark grey. During field surveys, extremely few SC buildings were found to possess seismic structures, such as structural columns and ring beams. These buildings do not fully meet the SP standard and are suspected to be below the SP standard. Their texture boundaries appear relatively distinct in the RS images.

(2) A relatively uniform plan and layout can be observed for the streets within the blocks in the RS images. Buildings showing similar texture patterns and colours in a polygon are uniformly classified as government-subsidised (GS) buildings. These buildings are constructed by the government according to the Standard for Seismic Fortification of Buildings and are therefore considered to meet the SP standard.

(3) RUF areas are home to alternating seismically fortified and unfortified buildings of various forms. As seen in the RS images, of the buildings in RUF areas, those neighbouring thoroughfares are mostly multistorey structures, while those distant from thoroughfares are generally densely and irregularly distributed low-rise structures. These buildings are classified as RUF buildings. Field surveys show that the SP standard is met by multistorey RUF buildings adjacent to thoroughfares but not by densely and irregularly distributed low-rise RUF buildings.

Typical buildings were photographed during field surveys. Information obtained from the photographs was subsequently statistically summarised to establish a database on the ArcGIS platform as a standard for determining building SPs in these areas.

3. Methods for Calculating Building Areas

From the principles of statistics, a sample is representative of and reflects the population, and population attributes can be estimated and inferred by analysing the sample drawn. Under the condition that the sample sites were evenly

distributed in space and among administrative divisions, this paper proposes a relatively simple formula to calculate building area. The main considered factors in the formula are as follows: the building area can be quickly calculated after visually interpreting the RS imagery, a more accurate building area can be obtained, and others can obtain relatively accurate results using this formula in visual interpretation of RS imagery research. Based on these considerations, this paper proposes two equations to calculate urban, RUF, and rural building areas.

3.1. Method for Calculating Urban Building Areas. During visual interpretation, standards of different scales are used to extract building polygons from urban and rural areas. Considering factors such as the structural type, seismic fortification standard, and lateral stiffness of buildings [23, 24], urban buildings are classified into three types: low-rise buildings (i.e., buildings with 1–3 storeys), multistorey buildings (i.e., buildings with 4–6 storeys), and high-rise buildings (i.e., buildings with 7 storeys or more). Each building is treated as a zoning unit for extraction. The building area model is given as follows:

$$M_C = \lambda_i \times M, \quad (i = 1, 2, 3), \tag{1}$$

where M_C is the building area of an urban building, M is the polygon area obtained from the RS image, and λ_1, λ_2, and λ_3 are the sample survey coefficients for low-rise, multistorey, and high-rise buildings, respectively. The areas of low-rise, multistorey, and high-rise buildings in urban areas are calculated separately using this equation with the help of the ArcGIS Field Calculator.

To accurately obtain a reasonable sample survey coefficient λ_i that can be used to calculate urban building areas across the study area, field sample surveys were conducted to collect data for low-rise, multistorey, and high-rise buildings. The numbers of storeys determined during the surveys were subsequently fitted to yield the corresponding value of λ_i.

Here, multistorey buildings are used as an example. Multistorey buildings at 88 sites were surveyed to determine their numbers of storeys, which were subsequently fitted to yield λ_2 (5.32). Table 1 summarises the polygon areas, actual numbers of storeys, areas determined based on survey data (treated as the actual areas), and estimated areas at the survey sites. The polygon area referred to here is the area of a polygon obtained during visual interpretation, that is, the area of a building interpreted from remote-sensing images. The field-surveyed area was calculated by multiplying the number of storeys obtained in the field survey by the area of the corresponding polygon, and the estimated building area was calculated by multiplying the fitted multistorey building coefficient by the corresponding polygon area. Then, a linear correlation analysis was performed on the actual and estimated building areas. The reliability of the fitting coefficient was examined through correlation analysis. Figure 5 shows the correlation analysis results for the actual and estimated areas of the multistorey buildings at the survey sites. In the figure, the small blue dots represent the linear trendline, and the large blue dots represent the estimated building areas. An analysis of Figure 5 reveals a correlation coefficient of 0.92 between the areas of the multistorey buildings determined based on survey data and those estimated with λ_2. This finding suggests that building areas estimated with λ_i are strongly correlated with those determined based on the actual numbers of storeys and that λ_i can be used to calculate urban building areas across the study area.

3.2. Methods for Calculating Areas of Buildings at Rural and RUF Sites. Most buildings in rural and RUF areas appear to be sheet-like structures in the RS images and are thus difficult to extract as individual polygons. In this study, buildings in rural and RUF areas are extracted based on block outlines. In other words, the outline of one block is extracted as one polygon, the area of which is denoted by M.

$$M_S = \beta_i \cdot M + \sigma, \tag{2}$$

where M_S is the building area in a block in a rural or RUF area, β_i is the regression coefficient (i.e., the ratio of the building area in the block determined based on survey data to the block area determined through visual interpretation; $i = 1$, 2, and 3 for SC, GS, and RUF buildings, resp.), and σ is the error compensation coefficient for the areas of standalone buildings (e.g., the building polygon areas indicated by B in Figure 6). The areas of SC, GS, and RUF buildings are calculated separately using this equation with the help of the ArcGIS Field Calculator. The polygon area here refers to the area obtained by visual interpretation. That is, the area is one block interpreted on the RS image. The definition of the survey point in the RUF area is consistent with the sample point in this area.

Here, the method used to calculate the regression coefficient for uniform GS buildings, β_2, is described. β_2 is the average ratio of the GS building areas determined based on field survey data to the corresponding polygon areas, that is, the proportion of the area of a GS building block that is occupied by all the buildings within the block (see Figure 6). To ensure accuracy, the obtained value of β_2 is validated based on survey data obtained at 88 sites (see Table 2). Figure 7 shows the results of the statistical error analysis. In the figure, the blue dots indicate the percentages of building area, and the short, vertical lines are error bars, each with a standard deviation of 1. The two horizontal lines above and below the error bars correspond to 40% and 20% of the total building area, respectively. The standard deviation statistical analysis indicates that the β_2 value is within a reasonable range. The same method is used to calculate β_1 and β_3, and thus the process is not described again.

4. Result Analysis

4.1. Estimated Area Correction. Normal statistical analysis was conducted to estimate the frequency distribution with a known mean and standard deviation. To verify whether the accuracy of the building areas calculated by equations (1) and (2) met the requirements, another 88 sample sites were selected from 22 districts and counties across the entire

Table 1: Numbers of storeys and areas of multistorey buildings in urban areas.

No.	Polygon area (m^2)	Actual number of storeys	Actual building area (m^2)	Estimated building area (m^2)	No.	Polygon area (m^2)	Actual number of storeys	Actual building area (m^2)	Estimated building area (m^2)
1	851.7	6	5110.5	4531.3	45	1243.6	4	4974.3	6615.8
2	1415.8	6	8494.9	7532.1	46	552.9	4	2211.6	2941.5
3	1604.8	6	9628.8	8537.5	47	1038.7	5	5193.6	5526.0
4	1449.5	5	7247.5	7711.3	48	1069.5	6	6417.0	5689.7
5	1471.9	4	5887.5	7830.3	49	1302.3	6	7813.6	6928.1
6	1146.7	5	5733.6	6100.6	50	759.9	6	4559.5	4042.8
7	997.2	6	5983.0	5304.9	51	750.2	4	3000.8	3991.1
8	774.5	5	3872.5	4120.3	52	1475.1	5	7375.4	7847.4
9	618.4	5	3092.0	3289.9	53	1395.9	5	6979.5	7426.2
10	1467.2	6	8803.4	7805.7	54	1009.8	6	6058.9	5372.2
11	1112.0	4	4447.9	5915.8	55	744.9	4	2979.4	3962.6
12	784.2	4	3136.8	4171.9	56	2668.9	5	13344.4	14198.4
13	1431.2	6	8587.0	7613.8	57	917.3	5	4586.6	4880.2
14	797.4	6	4784.4	4242.1	58	1243.4	6	7460.4	6614.9
15	1257.3	6	7543.8	6688.8	59	868.9	6	5213.7	4622.8
16	1025.4	5	5126.8	5454.9	60	517.5	6	3104.7	2752.9
17	1261.5	5	6307.5	6711.2	61	2663.7	5	13318.7	14171.1
18	1061.1	4	4244.5	5645.2	62	1406.2	5	7031.0	7480.9
19	513.5	5	2567.7	2732.1	63	722.5	4	2889.8	3843.5
20	834.2	6	5005.1	4437.8	64	966.2	6	5797.4	5140.3
21	695.8	6	4174.8	3701.6	65	981.9	4	3927.5	5223.6
22	775.5	6	4652.7	4125.4	66	1445.9	6	8675.7	7692.4
23	1012.3	5	5061.7	5385.7	67	1488.3	6	8930.1	7918.0
24	1857.0	5	9285.0	9879.3	68	1219.5	6	7316.9	6487.7
25	1068.5	6	6411.2	5684.6	69	861.7	5	4308.3	4584.0
26	1285.5	4	5142.0	6838.9	70	1051.4	6	6308.5	5593.5
27	947.7	6	5686.3	5041.8	71	1350.6	6	8103.6	7185.2
28	629.5	6	3777.1	3349.0	72	1233.0	4	4932.2	6559.8
29	1022.9	5	5114.4	5441.7	73	1004.5	4	4018.1	5344.0
30	1149.0	6	6894.1	6112.8	74	1033.0	5	5165.2	5495.8
31	1266.0	5	6330.0	6735.1	75	1347.3	6	8084.0	7167.8
32	1032.4	5	5161.8	5492.1	76	727.3	6	4364.0	3869.4
33	1258.8	6	7552.9	6696.9	77	1218.4	4	4873.7	6482.1
34	1254.2	6	7525.1	6672.2	78	1224.9	6	7349.4	6516.5
35	779.4	6	4676.1	4146.2	79	926.9	6	5561.4	4931.1
36	1038.1	4	4152.3	5522.6	80	1019.9	5	5099.5	5425.8
37	616.4	4	2465.7	3279.3	81	1248.8	5	6244.1	6643.8
38	616.9	6	3701.2	3281.8	82	860.7	6	5164.3	4579.1
39	1363.8	5	6819.1	7255.5	83	1038.3	6	6229.5	5523.5
40	1090.8	6	6544.7	5803.0	84	784.1	4	3136.3	4171.3
41	670.8	5	3353.8	3568.4	85	935.0	6	5610.1	4974.3
42	1036.8	6	6220.8	5515.8	86	610.8	6	3664.7	3249.4
43	1258.9	6	7553.6	6697.5	87	1094.1	6	6564.3	5820.4
44	1051.0	6	6305.8	5591.2	88	1910.9	5	9554.5	10166.0

Ningxia area for field surveys to verify the reliability and accuracy of the calculated building areas. The results indicated that the calculated building areas had an accuracy of 90%. The results of normal statistical analysis are shown in Figure 8.

The main influencing factors limiting the accuracy are as follows. First, the accuracy of visual interpretation varies among people. Second, some of the RS images are satellite images captured in the second or third quarter, which makes building boundaries difficult to interpret because of the occlusion of trees, thus resulting in an inaccurate acquisition of polygon boundaries.

4.2. SP Estimates. The building SPs in all the CLDs of Ningxia were preliminarily determined by visually interpreting the RS imagery. Subsequently, at least one sample site was surveyed in each village and township in all 22 CLDs of Ningxia. During field surveys, the building SPs at the survey sites were determined based mainly on three factors: (1) the SP data for the survey sites obtained from the local construction authorities, (2) the external appearance and structural features of the buildings (i.e., whether the buildings were equipped with seismic structures such as structural columns and ring beams), and (3) feedback from the occupants with respect to whether seismic measures

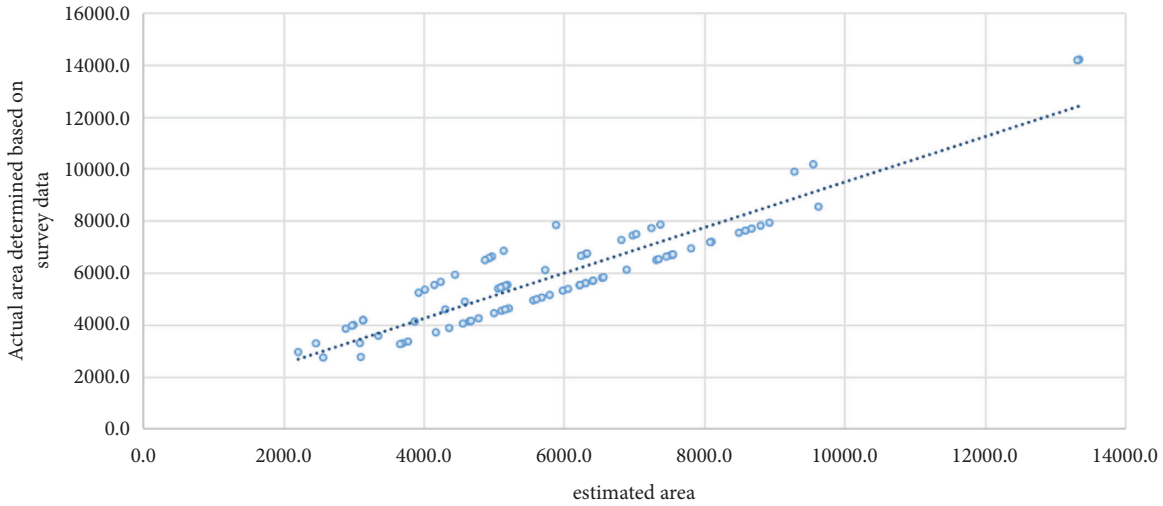

Figure 5: Correlation analysis of actual and estimated building areas.

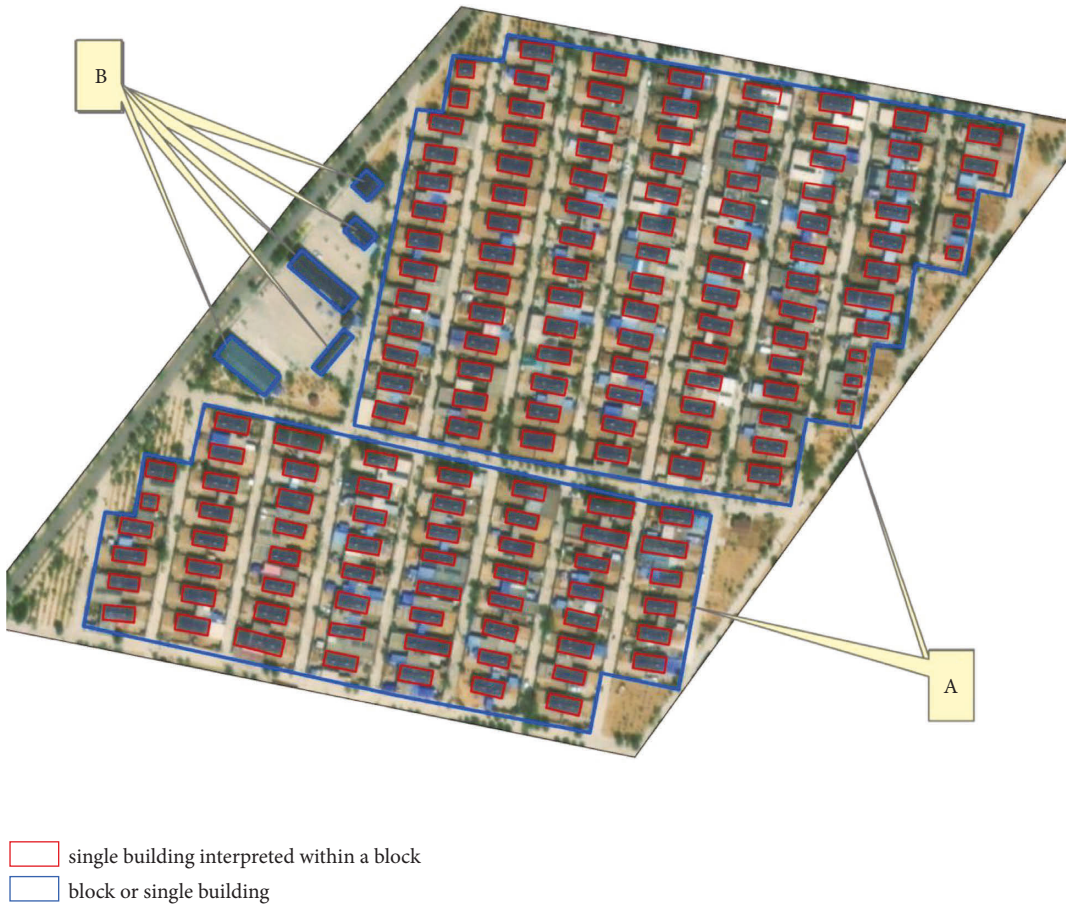

Figure 6: Visually interpreted GS building block and standalone building polygons.

were implemented during construction. The error correction of the original SP results was carried out based on the field survey results. The SP accuracy in Table 3 refers to the percentage of the sample sites in which the SP based on visual interpretation and the SP based on field survey data at the sample site are consistent. Here, the sample site is a zoning unit displayed by a building in the urban area or a block in the rural or RUF areas on a remote-sensing image. The results contain the following information. The SP accuracy is greater than 80% for Yuanzhou District, Xiji County, Delong County, Jingyuan County, Pengyang County, Haiyuan County, Hongsibu District, Tongxin

Table 2: Proportions of the areas of GS buildings determined based on field survey data.

No.	Polygon area (m^2)	Actual building area (m^2)	Proportion of the building area (%)	No.	Polygon area (m^2)	Actual building area (m^2)	Proportion of the building area (%)
1	29603	7844	26.5	45	17196	5346	31
2	38537	13600	35.2	46	5674	2040	36
3	21714	10304	47.6	47	30500	9216	30.3
4	20643	5632	27.2	48	11571	3025	26.1
5	3820	987	25.9	49	17083	6109	35.8
6	7872	2538	32.1	50	11470	3552	31.1
7	2372	905	38.2	51	18869	4508	24
8	7998	2576	32.1	52	33812	10452	30.8
9	2257	846	37.5	53	8395	1168	13.9
10	2047	820	40	54	118826	24750	20.8
11	43994	13776	31.3	55	11587	3380	29.1
12	18170	6960	38.3	56	3805	882	23.1
13	4428	1008	22.8	57	4872	1755	36.1
14	7855	2565	32.6	58	9829	2700	27.6
15	6904	1980	28.6	59	21014	6975	33.2
16	5561	1755	31.5	60	1853	715	38.6
17	13685	4925	35.9	61	106230	34182	32.1
18	5070	1708	33.8	62	12199	3300	27
19	13971	4416	31.7	63	3053	1170	38.4
20	858	354	41.3	64	59944	15860	26.5
21	15366	2808	18.2	65	231045	45770	19.8
22	66359	17157	25.8	66	7012	1854	26.4
23	33167	6270	18.9	67	21612	8228	38.1
24	51630	8580	16.6	68	4299	1096	25.4
25	24665	5278	21.4	69	23105	4255	18.4
26	4147	1331	32.2	70	1093	532	48.5
27	7186	2560	35.6	71	66524	8316	12.5
28	4214	1716	40.6	72	35280	8142	23.1
29	6124	1785	29.2	73	34830	5940	17.1
30	24279	7875	32.5	74	38649	7200	18.6
31	11680	2768	23.8	75	27292	7458	27.3
32	28288	4284	15.2	76	23203	6528	28.1
33	54917	20790	37.8	77	30596	7920	25.9
34	16505	2575	15.5	78	18319	4004	21.9
35	24317	8556	35.2	79	48775	15750	32.3
36	145650	33060	22.7	80	23021	6555	28.5
37	41683	14896	35.6	81	42684	15228	35.8
38	17948	6407	35.8	82	6920	1764	25.5
39	3193	1000	31.2	83	14928	4826	32.4
40	2459	852	34.8	84	19870	8370	42.3
41	39456	11808	30	85	28199	8140	28.9
42	14554	4321	29.7	86	8947	2976	33.2
43	5660	2028	35.9	87	10307	2728	26.5
44	10147	2662	26.2	88	5129	1800	35.2

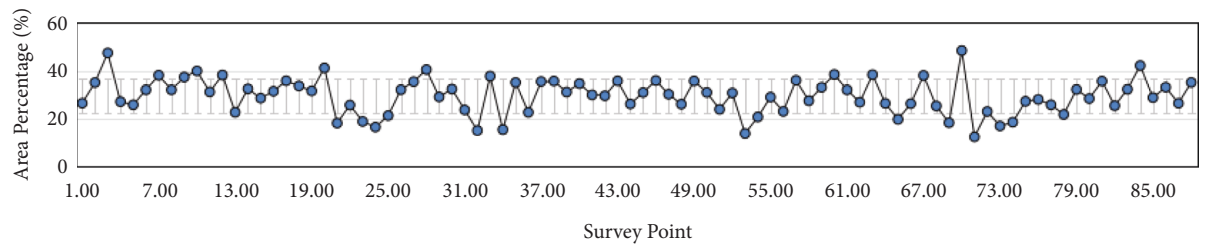

Figure 7: Proportions (in percentage) of the building areas at the survey sites to the corresponding polygon areas.

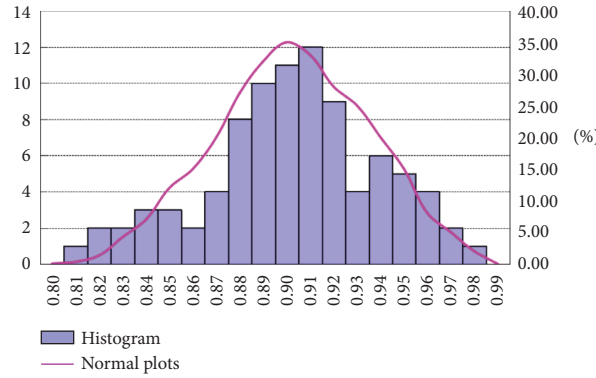

Figure 8: Normal distribution of the accuracy of the area estimates.

Table 3: Sample verification of building SPs.

No.	Name	Number of sample points	SP accuracy (%)
1	Xingqing District	16	70.7
2	Jinfeng District	7	71.4
3	Xixia District	8	75
4	Helan County	9	67.7
5	Yongning County	13	77
6	Lingwu City	13	84.6
7	Dawukou District	11	72.7
8	Huinong District	13	69.2
9	Pingluo County	26	76.9
10	Litong District	15	80
11	Hongsibu District	10	90
12	Yanchi County	12	75
13	Tongxin County	25	88
14	Qingtongxia City	20	80
15	Yuanzhou District	42	90.5
16	Xiji County	27	85.2
17	Longde County	15	86.7
18	Jingyuan County	10	90
19	Pengyang County	23	82.6
20	Shapotou District	23	74
21	Zhongning County	8	75
22	Haiyuan County	10	80
	Average	16	76

County, Qingtongxia City, Litong District, and Lingwu city (50% of all the CLDs). The SP accuracy is greater than 70% for 20 (91%) of the 22 CLDs. The SP accuracy is considerably higher for the CLDs in southern Ningxia than for Xingqing, Jinfeng, and Xixia Districts and Yongning and Helan Counties under the jurisdiction of Yinchuan City and Pingluo County and Huinong and Dawukou Districts under the jurisdiction of Shizuishan City. Based on the field survey results, this significant difference can be mainly ascribed to the following factors. First, buildings in the CLDs of northern Ningxia are complex and varied. Here, seismically fortified buildings alternate with unfortified buildings. As a result, interpreting the corresponding RS images is difficult and prone to errors. Figure 9 shows the distribution of SP accuracy for the buildings across the study area. Second, the RS images do not have a high spatial resolution; thus, some building SPs are difficult to accurately determine. Third, for the RUF buildings, using block-based acquisition in SP determination tends to ignore buildings with a certain SP that account for a relatively small proportion within a block.

4.3. Distribution Pattern of Building SPs. Based on the area and SP estimates, ArcGIS spatial analysis was used in this study to analyse the correlations between spatial location and SP attributes of buildings throughout the Ningxia region. The basic process of ArcGIS spatial analysis is as follows.

Spatial join analysis is a method that joins attributes from one feature to another based on the spatial relationship. Target features and the joined attributes from the join features are written to the output feature class. We used "many-to-one" to associate the join features with the target features. The join features were buildings, and the target features were CLDs (consisting of districts, county-level cities, and counties). The Match Option of different buildings in one CLD was set to the CLD.

Overall, the proportion of buildings with the required SP in each CLD is higher in northern Ningxia than in southern Ningxia, while the proportion of the buildings with substandard SP in each CLD is appreciably higher in southern Ningxia than in northern Ningxia, as shown in Figure 10. An analysis of the field survey results identifies two factors primarily responsible for the high proportion of buildings with substandard SP in southern Ningxia: (1) The efforts of nearly four decades of resettlement and nearly a decade of targeted poverty alleviation have improved the living environment and rural buildings in southern Ningxia. However, earlier government poverty alleviation efforts were mainly dedicated to substantially ameliorating rural buildings in terms of safety and comfort and failed to consider their SP. Most rural buildings with the required SP have been constructed in the last decade. (2) New and old buildings generally coexist in rural areas, presenting a certain challenge to the determination of building SPs and, therefore, the classification of buildings based on their SP.

Figure 11 shows the overall distribution of the buildings with the required SP, suspected substandard SP, and substandard SP, as obtained using the ArcGIS spatial analysis method; the figure reveals the following features. Buildings with the required SP are predominantly clustered in urban

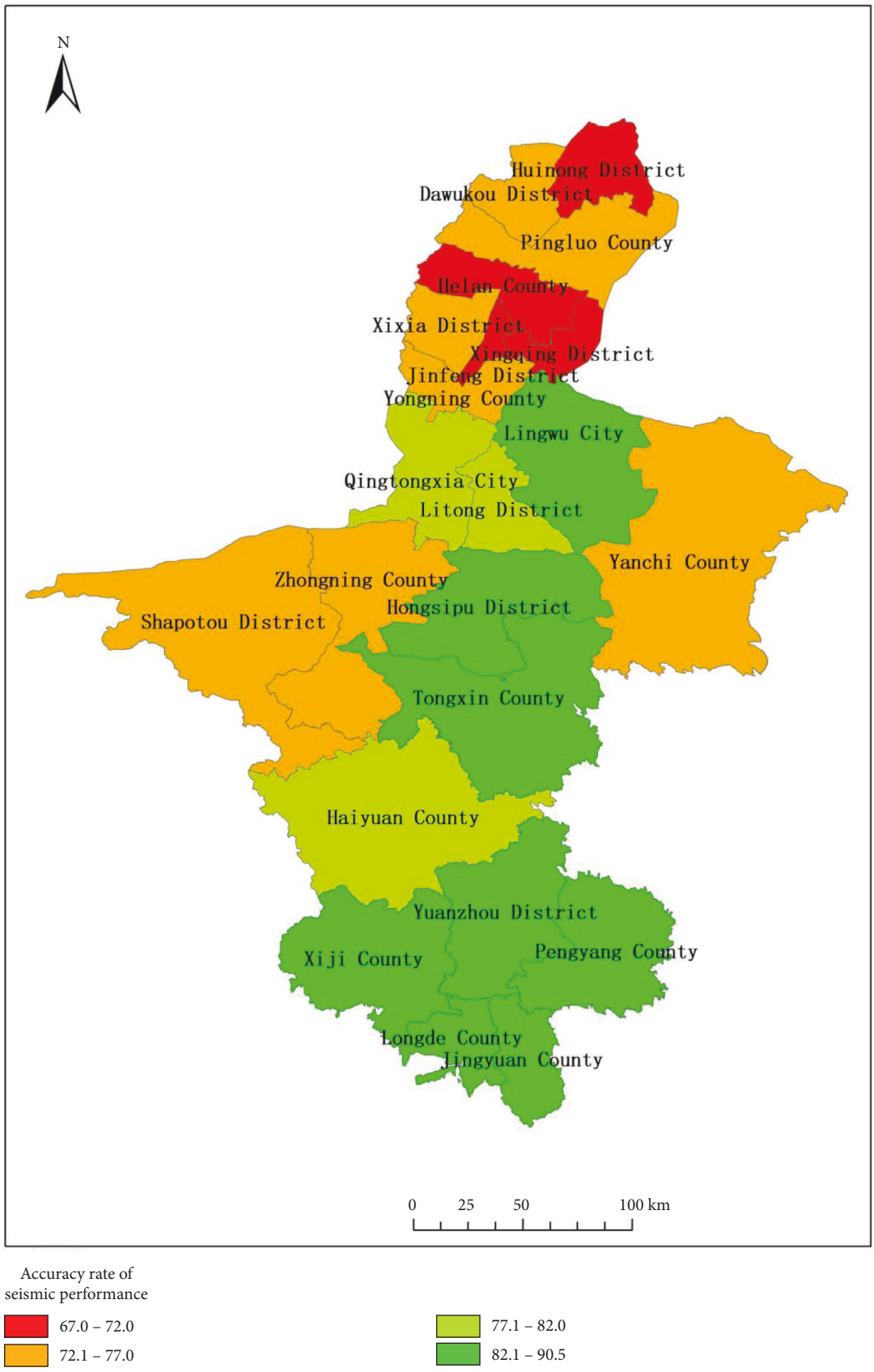

Figure 9: Distribution of the SP accuracy for the buildings across the study area.

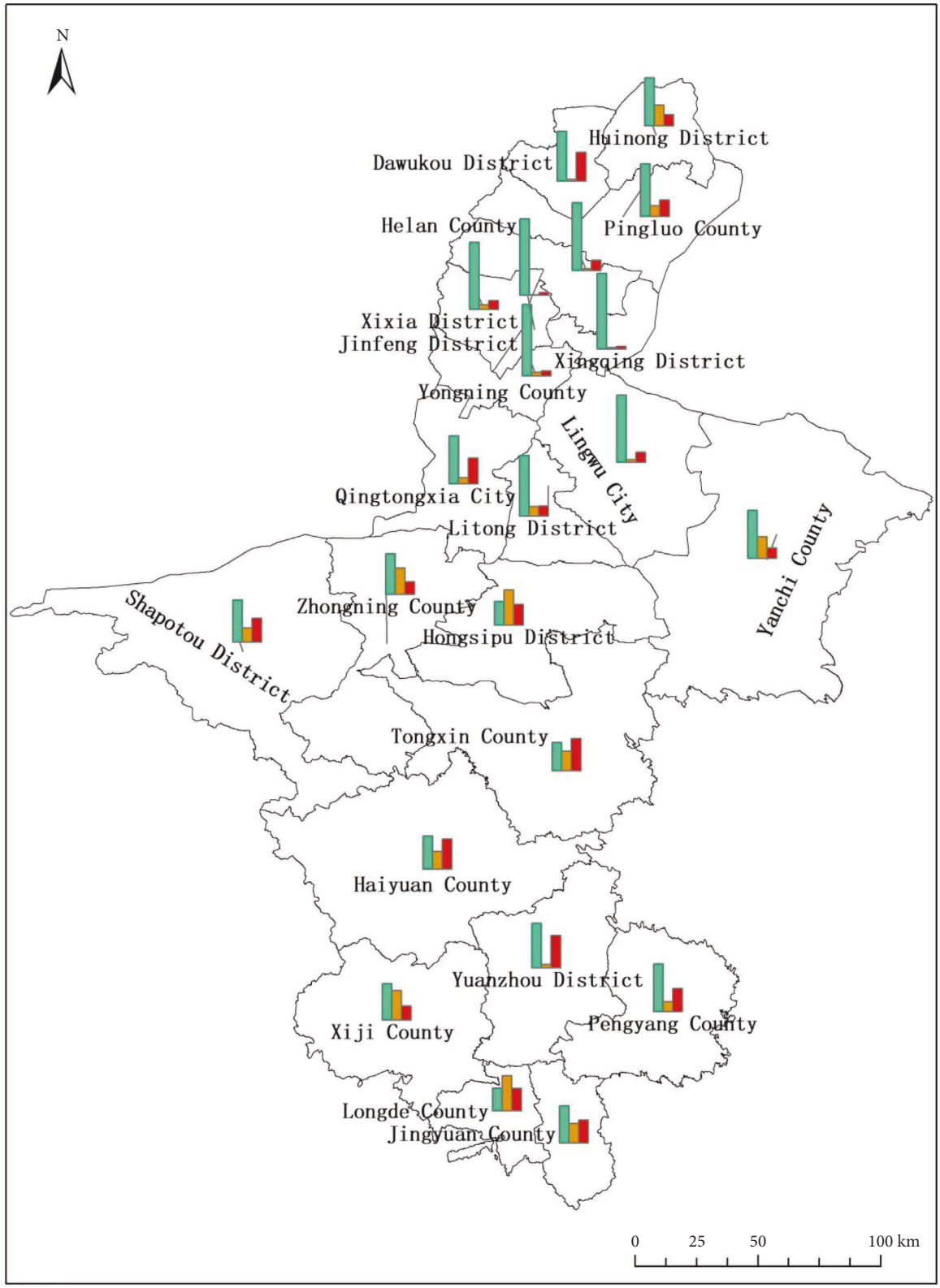

Figure 10: Proportions of the buildings in the three SP groups.

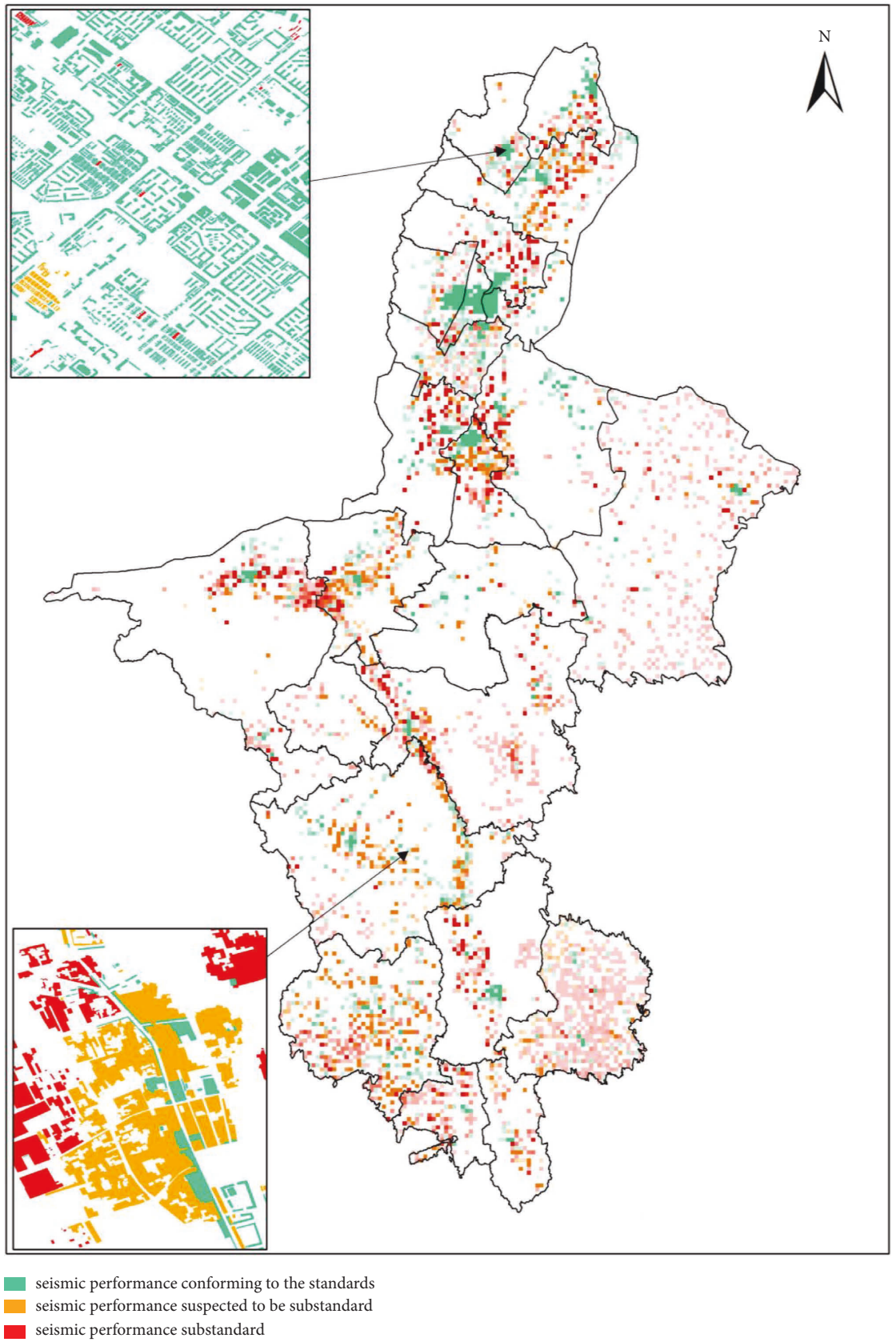

Figure 11: Distribution of the SP of the buildings among the three SP groups.

areas, with only a few distributed in villages and townships. Buildings with a suspected substandard SP and substandard SP are distributed mainly on the outskirts of urban areas and in the residential areas of villages and townships. This finding conforms to the field survey results. An analysis of the building SPs across Ningxia determined based on visual interpretation reveals generally high levels of SP in urban buildings and relatively low levels of SP in rural buildings.

5. Conclusion and Discussion

RS technology can be used to examine the SP and seismic vulnerability of building groups. Assessing the SP of buildings before earthquakes can save time and labour and produce timely data. This study presents a set method for extracting building area attributes and determining the SP of buildings that involves identifying building features in high-resolution RS images and statistical analysis of field sample survey results. The conclusions of this study are summarised as follows:

(1) Urban buildings are first classified based on the number of storeys into three types: low-rise buildings (i.e., buildings with 1–3 storeys), multistorey buildings (i.e., buildings with 4–6 storeys), and high-rise buildings (i.e., buildings with 7 storeys or more). Each building is treated as a zoning unit for polygon identification. The values of the fitting coefficients λ_1, λ_2, and λ_3 are determined based on sample survey data. Subsequently, the areas of low-rise, multistorey, and high-rise buildings are calculated by directly multiplying their polygon areas by λ_1, λ_2, and λ_3, respectively. Correlation analysis reveals a strong correlation between the areas estimated using this method and determined based on sample survey data, suggesting that this method can be used to calculate urban building areas.

(2) For rural and RUF areas, the outline of a block is treated as a zoning unit for visual interpretation. An equation is established to estimate building areas. Building areas estimated with β_i and subsequently checked and corrected based on field sample survey results follow a normal distribution.

(3) The SP estimates are validated based on data collected at one or more sample sites in each village and township in all 22 CLDs of Ningxia. The results show an SP accuracy greater than 80% for 50% of the CLDs and an SP accuracy greater than 70% for 20 CLDs, suggesting that the SP estimates are satisfactory.

(4) Based on the SP estimates, the ArcGIS spatial analysis method was used to determine the distribution of the buildings in the three SP groups across Ningxia. The results reveal the following features. Buildings with the required SP are clustered in the urban areas of each CLD, with a few distributed at the seats of the village and township governments. Buildings with a suspected substandard SP are distributed predominately in RUF areas and at the seats of the village and township governments. Buildings with a substandard SP are clustered in urban villages and RUF and rural areas. The field survey results lend concrete credence to the correctness and reliability of this analysis.

To summarise, the methods for determining building SP and calculating building area proposed in this study provide new ideas and approaches to solving the problem of identifying building SPs on a large scale. Ningxia is an earthquake-prone region that has experienced numerous destructive earthquakes, all of which caused many casualties and much damage. The available findings of seismic activity tectonic studies indicate that the region faces a high seismic risk. The results of this study play a guiding role in the seismic strengthening of buildings in the region by screening buildings with substandard SP.

In addition, despite the extensive research on applying RS technology in a postearthquake disaster assessment, few studies have applied RS images to evaluate preearthquake building SP on a large scale. This study has the advantages of high output efficiency, low input cost, and the ability to carry out a large-scale evaluation of building SPs. The research findings enrich the applied research on RS technology in the prevention and control of preearthquake risks and provide new ideas and new means for evaluating building SPs.

RS images are the basis for this analysis. To produce reliable results, RS images obtained during the same period that have sufficiently high resolution and are representative of the current situation should be used for the same region. The ages of buildings in a region can also be approximated based on their polygon features, positions, and spatial combinations in high-resolution RS images in conjunction with the regional characteristics to improve the accuracy of SP estimates. An overlay of the temporal and spatial distribution patterns of the population and buildings in a region can be used to quickly assess the impact of earthquakes of different magnitudes, such as potential economic losses and the number and distribution of casualties. All these areas warrant in-depth discussion and investigation.

Data Availability

The data of the remote-sensing images used in this study are from GF-2 satellite.

Conflicts of Interest

The authors declare that they have no conflicts of interest.

Acknowledgments

This study was supported by the (1) National key R&D Program of China (no. 2017YFB0504104) and (2) the First National Survey on Natural Disaster Risk (the Project on Seismic Risk Investigation and Elimination of Major Hidden Dangers of Ningxia).

References

[1] L. L. Xie and J. F. Zhang, "Application of satellite remote sensing technology in earthquake disaster reducation," *Journal of Natural Disasters*, vol. 9, no. 4, pp. 1–8, 2000.

[2] H. Wu, Z. P. Cheng, W. Z. Shi, Z. L. Miao, and C. C. Xu, "An object-based image analysis for building seismic vulnerability assessment using high-resolution remote sensing imagery," *Natural Hazards*, vol. 71, no. 1, pp. 151–174, 2014.

[3] P. Gueguen, C. Michel, and L. LeCorre, "A simplified approach for vulnerability assessment in moderate-tolow seismic hazard regions: application to Grenoble (France)," *Bulletin of Earthquake Engineering*, vol. 5, no. 3, pp. 467–490, 2007.

[4] M. Mueller, K. Segl, U. Heiden, and H. Kaufmann, "Potential of high-resolution satellite data in the context of vulnerability of buildings," *Natural Hazards*, vol. 38, no. 1-2, pp. 247–258, 2006.

[5] H. S. B. Duzgun, M. S. Yucemen, H. S. Kalaycioglu et al., "An integrated earthquake vulnerability assessment framework for urban areas," *Natural Hazards*, vol. 59, no. 2, pp. 917–947, 2011.

[6] S. Valero, J. Chanussot, and P. Gueguen, "Classification of basic roof types based on VHR optical data and digital elevation model," in *Proceedings of the IEEE International Geoscience and Remote Sensing Symposium*, Boston, MA, USA, July 2008.

[7] H. Wu, L. Zhou, X. Chi, Y. Li, and Y. R. Sun, "Quantifying and analyzing neighborhood configuration characteristics to cellular automata for land use simulation considering data source error," *Earth Science Informatics*, vol. 5, no. 2, pp. 77–86, 2012.

[8] H. Wu, Y. Sun, W. Shi, X. Chen, and D. Fu, "Examining the satellite-detected urban land use spatial patterns using multidimensional fractal dimension indices," *Remote Sensing*, vol. 5, no. 10, pp. 5152–5172, 2013.

[9] C. Gei and H. Taubenbock, "Remote sensing contributing to assess earthquake risk: from a literature review towards a roadmap," *Natural Hazards*, vol. 68, no. 1, pp. 7–48, 2013.

[10] M. Pittore and M. Wieland, "Toward a rapid probabilistic seismic vulnerability assessment using satellite and ground-based remote sensing," *Natural Hazards*, vol. 68, no. 1, pp. 115–145, 2013.

[11] D. Ehrlich, T. Kemper, X. Blaes, and P. Soille, "Extracting building stock information from optical satellite imagery for mapping earthquake exposure and its vulnerability," *Natural Hazards*, vol. 68, no. 1, pp. 79–95, 2013.

[12] Y. W. Zhao, C. Y. Hu, H. L. Shen, D. F. Ma, X. Li, and Y. G. Huang, "A hierarchical organization approach of multidimensional remote sensing data for lightweight Web Map Services," *Earth Science Informatics*, vol. 5, no. 1, pp. 61–75, 2012.

[13] X. Q. Wang, A. X. Dou, and L. Wang, "RS-based assessment of seismic intensity of the 2013Lushan, Sichuan, China MS7.0earthquake," *Chinese Journal of Geophysics*, vol. 48, no. 1, pp. 163–171, 2015.

[14] X. Fu, Q. Zhu, C. Liu et al., "Estimation of landslides and road capacity after august 8, 2017, MS7.0 jiuzhaigou earthquake using high-resolution remote sensing images," *Advances in Civil Engineering*, vol. 2020, pp. 1–11, Article ID 8828385, 2020.

[15] J. X. Guo, X. Y. Zhang, and J. Z. Ji, "A prelimimary study on the method of seismic intensity assessment based on residential building data and high resolution remote sensing images," *Seismology and Geology*, vol. 42, no. 4, pp. 968–980, 2020.

[16] L. Wang, X. Q. Wang, and X. Ding, "Study on loss assessment of construction earthquake damage based on remote sensing and GIS," *Earthquake*, vol. 27, no. 4, pp. 77–83, 2007.

[17] F. J. Zhao, S. Cai, and X. Chen, "Application of rapid seismic damage assessment based on remote sensing to Wenchuan earthquake," *Journal of Natural Disasters*, vol. 19, no. 1, pp. 1–7, 2010.

[18] "State Administration for Market Regulation&Standardization Administration of China," in *Seismic Ground Motion Parameters Zonation Map of China:GB18306-2015*, pp. 229-230, Standards Press of China, Beijing, 2015.

[19] *Ministry of Housing and Urban-Rural Development of the People's Republic of China & State Administration for Market Regulation, Code for Seismic Design of Building:GB50011-2010 (2016 Edition)*, vol. 6, no. 214, pp. 1–3, China Construction Industry Press, Beijing, 2010, in Chinese.

[20] C. Qiao, Y. Ding, X. Yongsen, Y. Yao, and H. Wang, "Image registration method based on geo-location information and precision analysis," *Acta Optica Sinica*, vol. 37, no. 8, Article ID 08280, 2017.

[21] *Ministry of Housing and Urban-Rural Development of the People's Republic of China & State Administration for Market Regulation, Standard for Classification of Seismic Protection of Building Constructions: GB50223-2008*, pp. 1-2, China Construction Industry Press, Beijing, China, 2008, in Chinese.

[22] "State Administration for Market Regulation&Standardization Administration of China," *The Classification of Earthquake Damage to Buildings and Special Structures:GB/T 24335-2009*, pp. 1–12, Standards Press of China, Beijing, China, 2009, in Chinese.

[23] J. F. Wang, *Research and Application of Extracting Building Anti-seismic Factors Based on Remote Sensing Technology*, Institute of Engineering Mechanics, CEA, 2021.

[24] S. H. Yu, Q. Y. Lei, and Y. Wang, "Study on high-precision static population spatial distribution in Xixia district, yinchuan," *Technology for Earthquake Disaster Prevention*, vol. 15, no. 4, pp. 757–766, 2020.